Subsurface imaging for panel paintings inspection: A comparative study of the ultraviolet, the visible, the Infrared and the terahertz spectra

ARTICLE *in* OPTO-ELECTRONICS REVIEW · JANUARY 2015

Impact Factor: 1.67 · DOI: 10.1515/oere-2015-0013

8 AUTHORS, INCLUDING:

S. Sfarra
Università degli Studi dell'Aquila
57 PUBLICATIONS **181** CITATIONS
SEE PROFILE

Clemente Ibarra-Castanedo
Laval University
140 PUBLICATIONS **1,032** CITATIONS
SEE PROFILE

Christophe Pradere
Institut de Mécanique et d'Ingénierie de Bo…
64 PUBLICATIONS **269** CITATIONS
SEE PROFILE

Jean-Christophe Batsale
MINES ParisTech
143 PUBLICATIONS **987** CITATIONS
SEE PROFILE

DE GRUYTER

OPTO-ELECTRONICS REVIEW **23**(1), 88–99

DOI: 10.1515/oere-2015-0013

Subsurface imaging for panel paintings inspection: A comparative study of the ultraviolet, the visible, the infrared and the terahertz spectra

A. BENDADA[1], S. SFARRA[*2], C. IBARRA-CASTANEDO[1], M. AKHLOUFI[3], J.-P. CAUMES[4], C. PRADERE[5], J.-C. BATSALE[5], and X. MALDAGUE[1]

[1]Computer Vision and Systems Laboratory, Department of Electrical and Computer Engineering, 1065 Av. de la Médecine Str., Laval University, Quebec City (Quebec), Canada, G1V 0A6
[2]Las.E.R. Laboratory, Department of Industrial and Information Engineering and Economics (DIIIE), 1 Piazzale E. Pontieri Str., University of L'Aquila, Loc. Monteluco di Roio – L'Aquila (AQ), I-67100 Italy
[3]Centre de Robotique et de Vision Industrielles (CRVI), 205 Rte Mgr-Bourget Str., Lévis (Quebec), Canada, G6V 6Z9
[4]ALPhANOV – Centre Technologique Optique et Lasers, Université Bordeaux 1, Bât. A11, 351 Cours de la Libération Str., 33405 Talence, France
[5]Laboratoire TREFLE, Esplanade des Arts et Métiers Str., 33405 Talence Cedex, France

Infrared (IR) reflectography has been used for many years for the detection of underdrawings on panel paintings. Advances in the fields of IR sensors and optics have impelled the wide spread use of IR reflectography by several recognized Art Museums and specialized laboratories around the World. The transparency or opacity of a painting is the result of a complex combination of the optical properties of the painting pigments and the underdrawing material, as well as the type of illumination source and the sensor characteristics. For this reason, recent researches have been directed towards the study of multispectral approaches that could provide simultaneous and complementary information of an artwork. The present work relies on non-simultaneous multi-spectral inspection using a set of detectors covering from the ultraviolet to the terahertz spectra. It is observed that underdrawings contrast increases with wavelength up to 1700 nm and, then, gradually decreases. In addition, it is shown that IR thermography, i.e., temperature maps or thermograms, could be used simultaneously as an alternative technique for the detection of underdrawings besides the detection of subsurface defects.

Keywords: near infrared reflectography, infrared thermography, ultraviolet, terahertz, panel paintings inspection, underdrawings/defects detection and characterization.

1. Research aims (secondary abstract)

Nondestructive and non-invasive assessment of surface and sub-surface defects is essential in cultural heritage inspection and nowadays many different technologies are available. Monitoring of artwork objects is not only useful to preserve historic memories but also a way to verify their degree of conservation. A non-simultaneous multi-spectral inspection using a set of detectors covering from the near to the long-wave IR is investigated herein. Supplementary results from ultraviolet, visible, and terahertz sensors are also presented for comparison purposes. The proposed approach has been applied on a sample that was fabricated respecting the rules described by the famous art master of the time such as Cennino Cennini (ca. 1370 – ca. 1440). Cennino Cennini describes a different type of underdrawing, made with graded tones rather than hatching for egg tempera. The use of imaging equipment working at different bands of the electromagnetic spectrum allows detecting possible degradation phenomena, providing in this manner of pertinent information about underdrawings, for example, *imprimatura* or *underpaintings*, and assuring repeatability of the measurements. For all these reasons, an inspection at different wavelengths is recommended.

2. Infrared reflectography for artwork inspection

2.1. Historical portray

IR reflectography have been investigated since the 1960s [1] although the origins can be retraced back to the 1930s as reported by Walmsley *et al*., (1994) [2], when IR photography was first proposed for the detection of underdrawings. Even though they are only sensitive to a relatively narrow IR spectral band (700–900 nm), photographic films are well suited for a few specific applications. For example, for the study of Flemish paintings of the 15th Century (medieval

*e-mail: stefano.sfarra@univaq.it

paintings) for which the painting layers are normally thin, and the oil medium and the painting pigments are semi-transparent in this IR range [3–5]. Nevertheless, restrictions on the spectral band and time delays (due to film development) limited the wide spread use of the technique.

It was not until the 1960s, after the work of Van Asperen de Boer [6,7], that vidicon cameras (900–2000 nm) first, and digital cameras (750–5000 nm) later, began to be routinely used by many recognized Art Museums [8–10]. It was in this period that the terms *IR reflectography* and *reflectograms* were first proposed [1]. According to Daffara *et al*. (2010) [3], vidicon cameras were still the most used device for IR reflectography in 2010, in spite of their limited spatial resolution, i.e., more than 100 images are required to properly (4×4 pixel/mm^2) reproduce a 1 m^2 panel painting. Furthermore, there are additional problems related to image mosaic reconstruction such as non-uniform illumination and image registration.

Commercial solid-state detectors such as charge-coupled devices (CCDs) make their appearance in the 1980s, with a near IR spectral resolution (700–1100 nm) slightly better than for photographic films. Complementary metal–oxide–semiconductors (CMOS) based on InGaAs (indium gallium arsenide, 750–1700 nm) or PtSi (platinum silicide, 750–5000 nm) detectors were developed in the 1990s, providing an extended IR spectral band.

The next generation of IR reflectography systems are the multispectral (up to 14 narrow spectral bands) single-point scanners, which considerably diminish the effects of optical and geometrical non-uniformities with respect to multi-detectors arrays [3,11].

The use of commercial IR cameras and the required accessories (lenses, filters, and light sources) is still an interesting alternative for artwork inspection given its straightforward deployment and lower cost compared to single-point scanners [12]. In this study, the use of several cameras working at different spectral bands combined with a set of filters and illumination sources is adopted as a non-simultaneous multispectral approach for panel painting analysis. Tests were carried out at five different institutions in three countries.

2.2. The principle

When exposing an object to a radiation source, e.g., a painting illuminated with a wide-spectrum (from ultraviolet to far IR) incandescent lamp as illustrated in Fig. 1, part of the radiation will be absorbed by, part will be transmitted through, and part will be reflected from the incident surface, depending on the radiation wavelength being observed. For instance, a visible camera will capture the light (in the visible spectrum 400–700 nm) reflected from the painting surface, providing information about colours and textures.

The near (NIR) and short-wave (SWIR) IR parts of the radiation, which contain practically no thermal emissions, can penetrate thin layers of painting before being reflected back to the surface from an non-absorbing medium such as the preparation surface (usually made of chalk and gypsum) whilst this same radiation will be absorbed by carbon based or other absorbing elements (underdrawings), if present. A NIR/SWIR camera would capture images showing the reflective and absorbing areas through relatively thin painting layers. Most of the oil paints used for panel painting

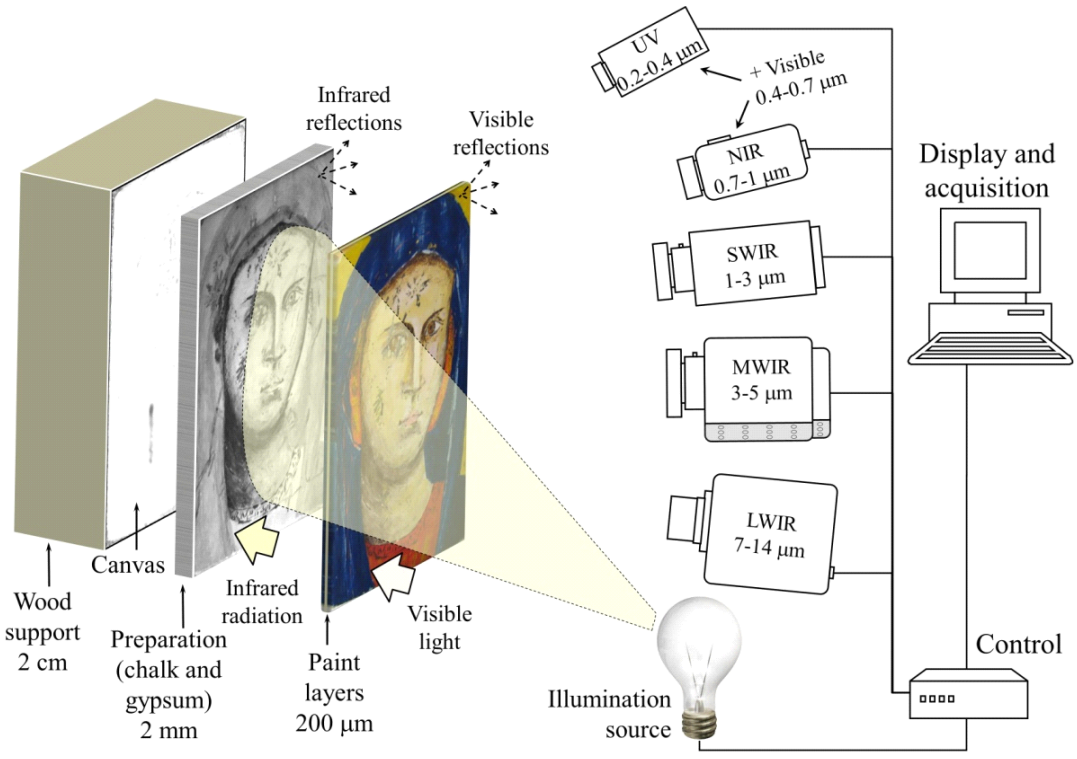

Fig. 1. Experimental setup for multi-spectral IR reflectography inspection of panel paintings.

(usually linseed oil with inorganic suspended oxide or mineral salt pigments [13]) are transparent to NIR/SWIR light, i.e., IR radiation in the near and short-wave IR can pass through thin painting layers containing such pigments; whilst carbon derivatives (such as graphite and charcoal) are opaque in this spectral regions, i.e., radiation is mostly absorbed by these elements. For instance, brown and gray are more transparent than some light colours, greens and blues are nearly opaque, whilst most black tones are even more opaque [13].

The transparency in the NIR/SWIR bands is a complex function of: (1) the optical characteristics of the pigment colour, (2) the underdrawing material, (3) the paint layer thickness (typically a fraction of millimeter [3]), and (4) the detector wavelength (transparency increases between 1000 and 2500 nm for different configurations [2], generally showing a peak near 2000 nm [7]). A NIR/SWIR camera can be used to reconstruct two-dimensional (2D) images, i.e., *reflectograms*, of the reflected light under the painting layers. Interesting applications include the detection of guiding sketches and signatures (opaque to NIR/SWIR radiation) drawn by the artist prior to the application of painting layers; the detection of hidden paintings (painters often use a previously painted canvas or change their mind during the painting progression), the monitoring of the restoration processes required on aging cultural heritage artworks, and the detection of intentional and unintentional alterations.

In this paper, the possibility of detecting underdrawings using sensors working at other infrared bands will be studied. For instance, the mid- and long-wave infrared spectra are examined. Some results are presented and discussed in Sect. 3.5.

2.3. Degradation factors in artworks

A natural altering factor for ancient artworks is obviously aging. However, their integrity and durability can vary significantly depending on a variety of aspects, such as improper selection of materials, conservation accidents and unnecessary or unprofessional treatment [14]. Panel paintings are composite structures incorporating wood, hidden glue, gesso composed of glue and gypsum (calcium sulfate) or chalk (calcium carbonate), paints and resin varnishes. Paint media can include wax, egg tempera, oils, and their combinations [15]. Panel paintings structure can also vary in complexity, the simplest consisting of paint applied directly to wood [14,15]. According to the rules of Italian ateliers in the 13th and 14th centuries, the canvas is glued to the wood, and then a gesso ground is applied above the canvas as a basis for paints and varnish. Therefore, panel paintings can be considered a layered structure [16]. Fluctuations in ambient parameters can cause elastic and/or plastic deformations: these different expansions and contractions experienced by different regions of the layered structure produce anisotropic deformations, amplified by natural aging, which can alter the mechanical properties of each layer and eventually lead to the formation of detachments and cracks [14,15]. A frequent and dangerous damage is the formation of detachment regions, which can occur at any depth inside the structure [16]. These damages are often due to deformations of the support (less flexible with age), caused by humidity or temperature variations but may also be due to intrinsic factors such as irregular wood grain or structural anomalies.

The inspection of artworks in a safe and effective manner is thus required in order to assess their condition.

The wood panel painting studied herein, named the *Madonna*, consists of a 15 cm × 21 cm × 2 cm specimen of poplar wood. Poplar wood is soft, weak, fine grained and fine textured; it is diffused-porous and the pores are very small. A radial cut piece was used in the present case. A colour photograph is presented in Fig. 2.

The protocol of construction was based on the traditional techniques described by the famous art master of the time such as Cennino Cennini [16,17], and it included: (I) a study of the typical structure of the paintings to be simulated; (II) the determination of the deterioration factors that can be reproduced; (III) the definition of the defects that have to be reproduced; (IV) the construction of the sample; and, (V) the documentation and characterization of the model panel painting.

The study of the most typical defects found on panel paintings provided the necessary information for the selection of the most appropriate ones for the construction of the model sample. On the wooden support, a layer made of animal-skin glue, resin and canvas of linen (also known as "size") has been applied. Once the size dried, layers of gesso have been added. Each layer was sanded down before the realization of the next. At the end of the process, a smooth hard surface was realized. The design of the *Madonna* was laid out by charcoal, as well as the signature of the manufacturer. Thin sticks of vine charcoal, produced from willow wood, were also used for toning down areas, to create subtle shadows and sketches. Small brushes dipped in a mixture of pigment and egg yolk were adopted as method of application. Small strokes of brush were applied to define the final layout. The manufacturer also kept in mind that tempera dries quickly and is not conducive to mistakes, so each stroke was perfect each time. A layer of varnish completed the sample construction with the intent of protecting and prolonging the lifespan of the paint finish. Finally, four artificially detached regions (Mylar inserts) were inserted inside the layered structure as deeper discussed in Sect. 3.5.

Previous research works have been devoted to the assessment of this specimen using interferometric techniques [18,19], IR thermography [20,21], or a combination of both [22,23].

3. Non-simultaneous multispectral inspection results

For the present work, a non-simultaneous multispectral inspection of *The Madonna* specimen was performed, ranging from the ultraviolet [24] to the terahertz [25], on the operating spectral ranges of the eight cameras listed in Table 1. As

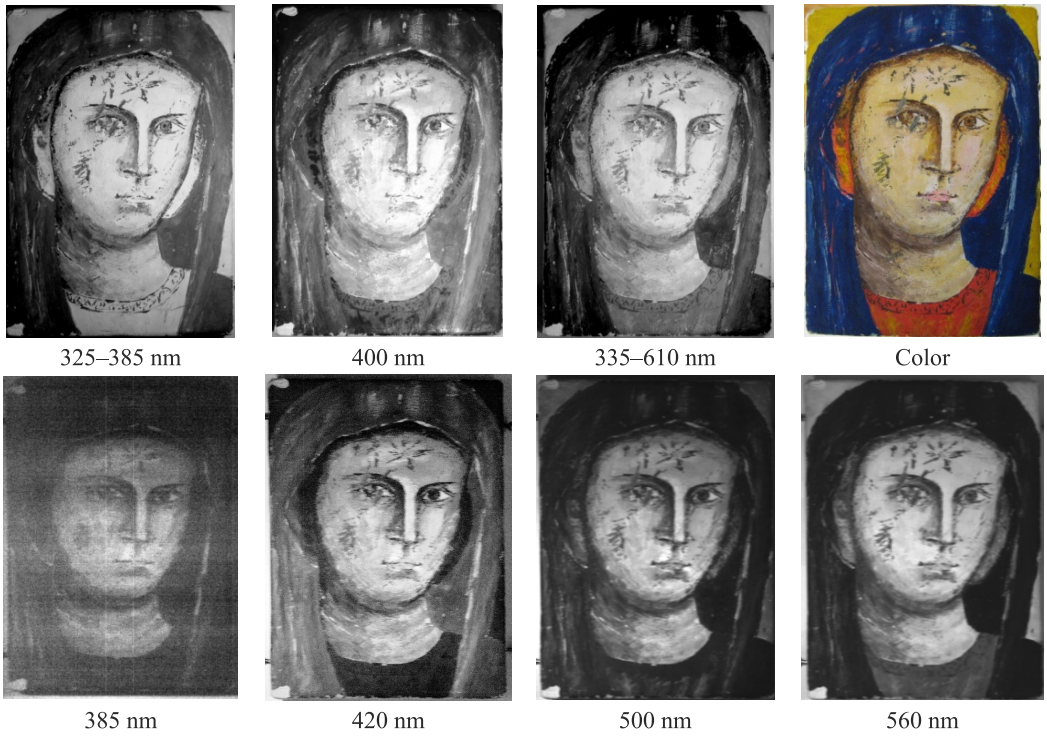

Fig. 2. Ultraviolet to visible spectrum images at different wavelengths obtained with the JAI UV camera UV-VIS and a colour photograph for reference (top row), and the imaging spectrograph HYPER (bottom row) for comparison.

Table 1. Cameras' types and operating spectral band.

Code	Camera type	Range	Brand and model	Optical filters and lenses	Sources
UV-VIS	Monochrome CCD	200–1000 nm	JAI CM-140GE-UV 1380×1040	UV band-pass filter: 325–385 nm UV band-pass filter: 325–610 nm	Halogen lamp 5000 K LED 400 nm
HYPER	Hyperspectral camera (spectral resolution = 2.8 nm)	400–1000 nm	Specim, ImSpector V10E Hamamatsu CCD camera C8484-05G 1344x1024	IR band-pass filter: < 780 nm	Halogen Lamp 5000 K
VIS-NIR1	Monochrome CCD	400–1000 nm	Mightex, BTN-B013-U 1280×1024	IR band-pass filters: 850 and 910 nm	Halogen Lamp 5000 K
VIS-NIR2	Monochrome CCD	400–1100 nm	µTech, Phoenix PC-1280 1280×1024	Visible cut-off (< 0.75 µm) IR cut-off (> 0.75 µm) 18 mm lens Red, green and blue filters	Incandescent wide spectrum LED 850 nm LED 940 nm
SWIR	CMOS, InGaAs Uncooled	900–1700 nm	Goodrich, SU640SDWH-1.7 RT 640×512	Narrow-band filters: 1300, 1430 and 1650 nm 55 nm lens (Nikkon) 50 mm lens (StingRay)	
MWIR1	CMOS, PtSb Cooled (liquid nitrogen)	3–5 µm	Santa Barbara, Phoenix-Mid 320×256	25 mm lens	Photographic flashes (Balcar)
MWIR2	Cooled (Stirling)	3–5 µm	FLIR, Phoenix-Mid, PtSb 640×512	25 mm lens	Photographic flashes (Balcar) Incandescent wide spectrum Heating plate Furnace
LWIR1	Microbolometer Uncooled	7.5–14 µm	Jenoptik, IR-TCM 384, microbolometer 384×288	12.5 mm lens	
LWIR2	Microbolometer Uncooled	7.5–13 µm	FLIR, S65, microbolometer 320×240	25 mm lens	IR lamps (SICCATHERM E27)
THz	Microbolometer Uncooled	0.11 THz (3,000 µm)	FLIR, A20, microbolometer 320×240 + THz thermal converter	34 mm lens	CW electronic GUNN diode

seen from this table, several optical filters were used in combination with different IR radiation sources in order to target specific narrow spectral bands, creating a database of more than 200 images. Details on the equipment used are also provided in for reference. In addition, two series of 1024 multispectral images, from 377 to 1020 nm, were acquired using the hyperspectral camera listed in Table 1. A comparison of images obtained for different wavelengths is discussed next.

3.1. Ultraviolet to visible spectrums (10 to 700 nm)

The top row of Fig. 2 presents 4 images of the *The Madonna* obtained with the UV camera (UV-VIS in Table 1) and a colour photograph for reference. There are some interesting observations that can be made from these images. First, with the exception of the 400 nm result, images are very similar, showing light brown tones bright (as in the skin) and blue tones dark (as in the headscarf), while red tones appear bright (as in the blouse) and yellow tones even brighter (as in the background). In the case of the 400 nm image however, blue and red tones have similar brightness (compare the headscarf to the blouse), light brown is still bright (e.g., the skin) but yellow tones are dark now (e.g., the background). Furthermore, the 325–385 nm image shows a slight indication of the author's signature (bottom-right), although this signature cannot be seen in the visible spectrum (colour photograph). Spectrographs obtained with the multispectral imaging spectrograph at similar wavelengths are also shown in the bottom row of Fig. 2. As the first observation, image quality is poor near the lower limit of the spectrograph spectrum, but it improves considerably for longer wavelengths. Besides that, these spectrographs show features similar to those found in the UV-VIS images and the colour photograph presented in the top row of this figure.

The 400 nm image (top row) and the 420 nm spectrograph (bottom row) were obtained in narrow-bands close to the visible spectrum, i.e., near the violet and indigo bands. For RGB digital processing this corresponds to the blue band (B). Hence, a colour analysis was also conducted to further explore these results.

3.2. Colour analysis

Grayscale images from the three primary colours: red, green and blue, were obtained using narrow-band spectral filters mounted on a CCD camera (VIS-NIR2 in Table 1), and are shown in Fig. 3. Special attention was given to avoid moving the camera and painting during the manipulations so the three grayscale images represent exactly the same features, pixel by pixel. A colour image was reconstructed under MATLAB, using these three images as channels red, green, and blue, respectively. The red (R) and green (G) band images in Fig. 3 are very similar to the UV images in Fig. 2 (with blue tones appearing dark whilst red, yellow and light brown tones are bright), with the exception of the 400 nm image as mentioned before which is closer to the blue band image (B) of Fig. 3. Gold tones appear very dark in the 400 nm (Fig. 2) and the B-band (Fig. 3) images as can be seen around the face (below the headscarf) from the right to the left ear, and also in the red blouse at the bottom of the painting. The gold painting around the right ear of *The Madonna* is better seen in the 400 nm image than in the B-band image though.

Furthermore, it is interesting to notice that the yellow background appear dark in the 400 nm image but bright in the B-band image which indicates that this yellow paint composition is significantly different from the gold painting referred before.

3.3. Near IR spectrum (700 to 1100 nm)

Figure 4 presents a series of reflectograms at different wavelengths ranging from the visible (400–700 nm) to the near IR (700–1100 nm) acquired with two CCD cameras (VIS-NIR1 and VIS-NIR2 in Table 1). The equivalent spectrographs obtained with the imaging spectrograph HYPER are included below each NIR reflectograph for comparison. In all cases, reflectograms show a considerably better spatial resolution than spectrographs though feature contrast follows the same trends for both image types.

The first image corresponds to the visible spectrum and was obtained with the VIS-NIR2 camera using a NIR cut-off filter, whilst the last 7 images were obtained with either

Red channel Green channel Blue channel Reconstruction

Fig. 3. Grayscale images colour reconstruction using grayscale red, green and blue images as three channels R, G, and B, respectively.

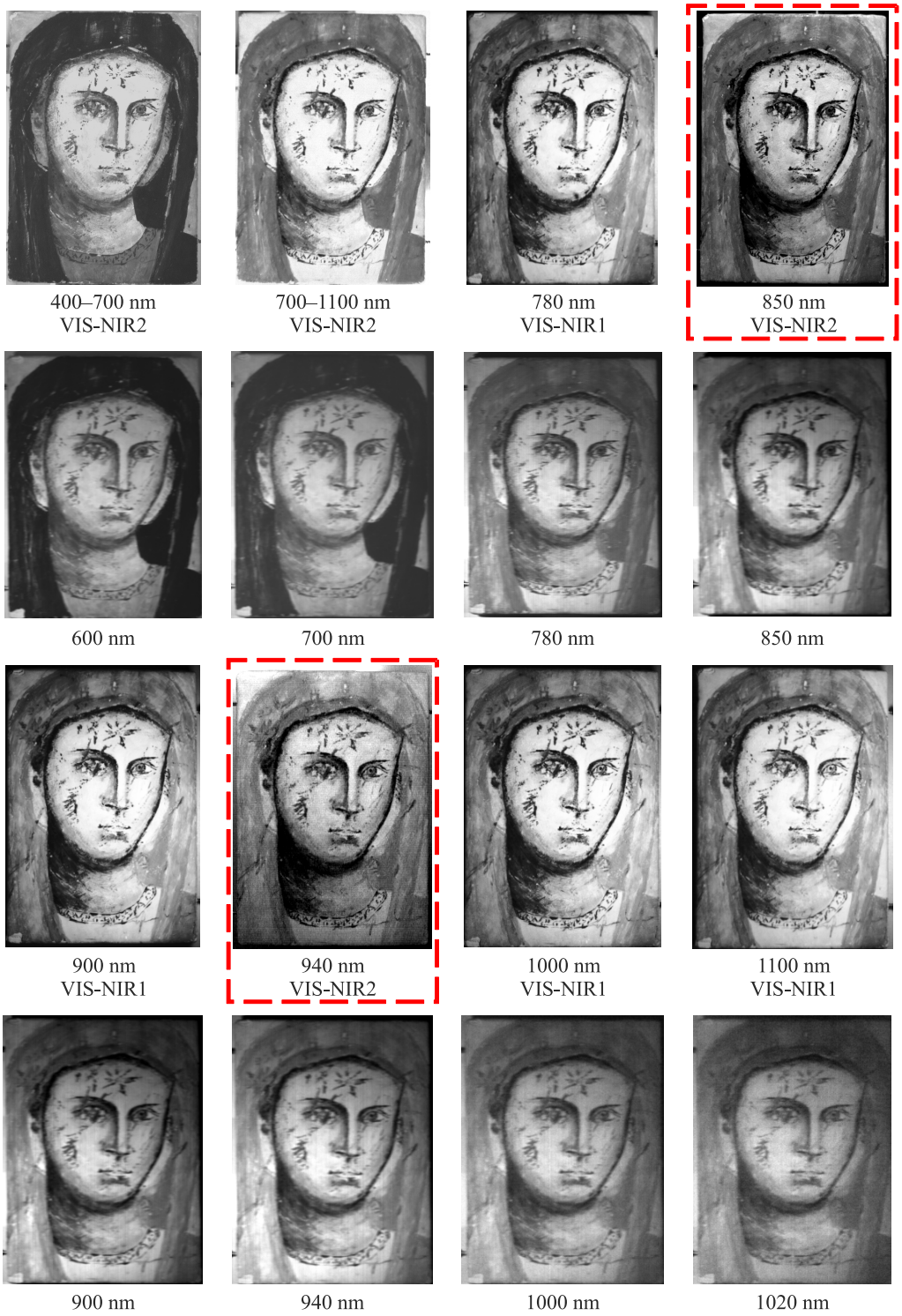

Fig. 4. Near IR reflectograms at different wavelengths (top) and spectrographs at equivalent wavelengths (bottom).

VIS-NIR1 or VIS-NIR2 cameras (as indicated in Fig. 4) using visible cut-off filters (only IR light was passing to the sensors). Specific wavelengths were obtained through the use of narrow-band-pass (NBP) filters. Images obtained at 850 nm and 940 nm (Fig. 4) marked with a dotted rectangle were obtained with LED projectors (illuminators).

There are several underdrawings and a series of inscriptions that are visible in the near IR which are identified in Fig. 5 (rightmost image). Starting at the top-left above the right ear of *The Madonna* and following the clockwise motion: ❶ a maple leaf, ❷ the inscription "CE" (inverted), ❸ a sort of bird, ❹ a small square, some ❺ sketches and ❻ unrecognizable symbols, some other sketches ❼ around the right eye and ❽ the neck, ❾ the author's signature, and what appears to be a ❿ false start for the neck.

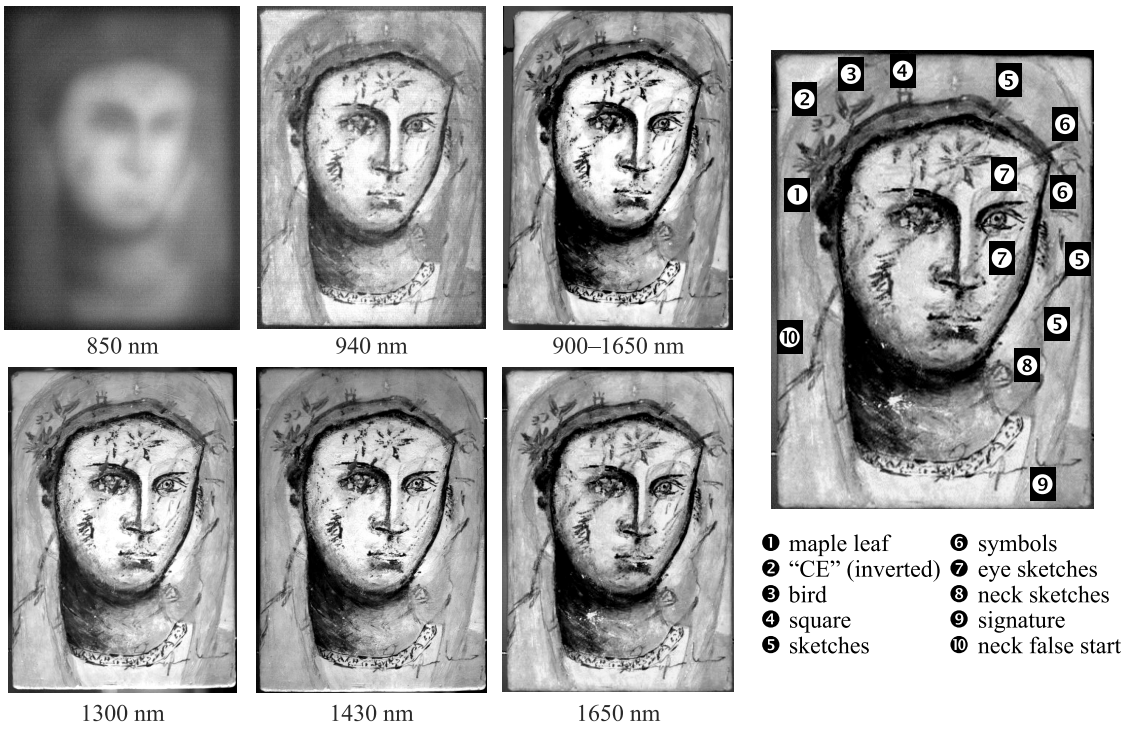

Fig. 5. Short-wave IR reflectograms at different wavelengths.

The underdrawings contrast improves with the wavelength up to approximately 940 nm. Practically, no change is observed after this wavelength. This is probably due to the operational spectral range of the CCD cameras for which the efficiency decreases sharply (< 60%) for wavelengths greater than 900 nm.

3.4. Short-wave IR spectrum (1100 to 3000 nm)

The SWIR camera has a quasi-constant quantum efficiency (~80%) from 900 nm to 1650 nm.

The first two images in Fig. 5 (top line) were acquired employing LED illuminators at 850.nm and 940.nm. The first image is extremely blurred because 850 nm corresponds to a spectral value below the SWIR camera's sensitivity wavelength range (see SWIR range in Table 1). The 940 nm reflectogram, even though is close to the lower boundary of the camera's operational spectral band, clearly shows most of the painting's underdrawings. These feature become even clearer in the last four reflectograms in Fig. 5 which were obtained under similar illumination conditions (wide spectrum light source) but either without any filter, as in the rightmost image in the top row (it covers the whole spectral operating band of the camera); or using narrow-band filters at different wavelengths (as indicated), as in the three reflectograms of the bottom row.

This led us to conclude that under-drawing contrast in the case of a short wave IR is primarily related to the detector efficiency and not to the wavelength.

As stated before, even though transparency in the NIR/SWIR bands is a very complex phenomenon, it has been observed that it usually increases from the near to the short-wave IR bands up to a peak near 2000 nm [2,7]. This trend was confirmed by the results in Fig. 4 and 5. Unfortunately, there is a gap between 1.7 μm and 3 μm for which no measurement equipment was available (see Table 1). Future research must be conducted in order to verify under drawing detectability in this spectral range.

3.5. Medium- and long-wave IR spectra (3 to 14 μm)

On the other hand, active IR thermography [26] experiments were carried out in parallel to inspect the sample for detection and characterization of subsurface defects, similar to the studies presented in Refs. 20, 21, and 22. In active thermography, the surface of the inspected sample is heated (or cooled) using an external source in order to produce a thermal contrast and a thermal camera (MWIR or LWIR) is used to display and record the temperature evolution on the surface. The experimental procedure is illustrated in Fig. 6.

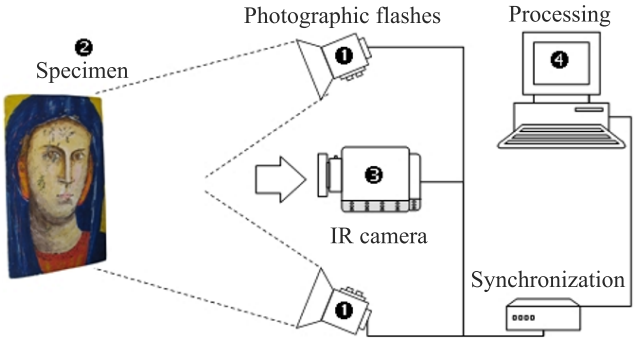

Fig. 6. Experimental setup for pulsed thermography.

There exist some differences between imaging in these bands. Measurements in LWIR are usually less sensitive to ambient illumination; conversely, MWIR band exhibits lower optical diffraction and background radiation, which give a sharper imaging with a better contract. In a normal measurement by thermography, a temperature estimation is performed based on IR radiation *emitted* from the surface. This means that *reflected* IR radiation should be reduced or carefully taken into account. Many objects at room temperature are good sources of IR radiation at thermal wavelengths and, therefore, no artificial illumination source is needed. As it is well known, the amount of emitted radiation depends both on the surface temperature and the surface total emissivity, i.e., its ability to emit energy by radiation. For an opaque object, under the graybody assumption, emissivity is also related to the surface ability in reflecting energy: objects with low emissivity are good reflectors. The spectral distribution of energy emitted by an object is given by the product of the Planck distribution for a given temperature with the emissivity of the object. In the vicinity of the room temperature (293 K), the Plank distribution has a maximum in the LWIR (around 10 μm); the peak in the MWIR is approximately one-fourth of this maximum. In terms of total energy emitted, it can be easily shown, by using the blackbody radiation functions, that a blackbody at 293 K emits only 1.1% of its energy in the MWIR band and about 42.4% in the LWIR band.

Surface heat distribution would be uniform for an object without defects whilst a thermal gradient will be observed if a defect is present on or under the surface. The time of appearance of defect is then related to its depth [26].

Active thermography is widely used in aerospace nondestructive testing (NDT) [27] and is constantly finding new applications, one of which is the inspection of cultural heritage objects and artworks [28–30]. As previously mentioned, *the Madonna* specimen [Fig. 7(a)] was originally conceived with four artificial internal defects (Mylar inserts) at different locations [Fig. 7(b)]. Several works have been dedicated to the detection of these defects using different NDT techniques [18–23]. Unfortunately, the information about the exact depths of the defects has been lost. However, in Ref. 21 the authors provide an estimated depth for defects A, B, C, and D by combining computer modelling and thermal tomography. At a later stage, in Ref. 23 the authors confirmed the previous results using the pulsed phase thermography (PPT) technique. The results obtained are summarized in Table 2 along with the defects' dimensions. In the case of pulsed thermography (PT), the specimen was inspected using different cameras (MWIR1, MWIR2 and LWIR1) and data were processed using the PPT algorithm [31,32]. In the case of camera MWIR1, the flashes were set to low power (0.4 kJ each flash) during the experiment in order to reduce the surface temperature (approximately 1.5 C rise in the average surface temperature [22]). Still, the choice of an IR camera with high temperature resolution has enabled the acquisition of thermograms of high quality.

Table 2. Defects' dimensions and depths according to Refs. 21 and 22.

Defect	Dimensions	Estimated depth range as reported in [21]	Estimated depth range as reported in [22]
A	D = 5 mm	0.3–0.8 mm	0.3–0.7 mm
B	28×4 mm	0.8–0.9 mm	0.5–1.1 mm
C	D = 8 mm	> 1.4 mm	0.7–1.6 mm
D	14×3 mm	> 2.0 mm	–

A result (*phasegram*, at $f = 0.075$ Hz) is shown in Fig. 7(c), where 3 of the defects: A, B and C can be clearly seen. It seems that defect D is located too deep to be detected by thermography. Fig. 7(d) presents a fusion between the colour photograph [Fig. 7(a)] and the phasegram [Fig. 7(c)].

PT experiments also allowed to detect the underdrawings as shown in Fig. 8 for 4 different cameras (MWIR1, MWIR2, LWIR1, LWIR2). As can be seen, under-drawings appear with fairly good contrast on these images, when either a mid- or a long-wave cameras were used. They appear more clearly at the beginning of the experiment, i.e., right after the specimen is heated with the photographic flashes and gradually

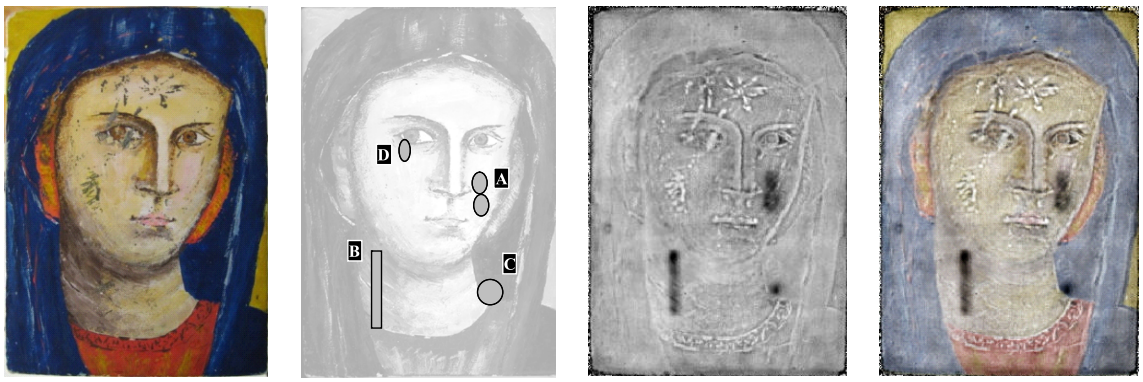

(a) (b) (c) (d)

Fig. 7. Subsurface artificial defects inspected by pulsed thermography: (a) colour photograph of the specimen; (b) image showing the localization of the 4 internal defects; (c) processed result obtained by pulsed phase thermography; and (d) composed image resulting from overlay of photograph in (a) and PPT result in (c).

(a) MWIR1 (b) MWIR2 (c) LWIR1 (d) LWIR2

Fig. 8. Mid- and long-wave IR thermograms obtained at early times, $t = 0.02$ s after pulsed heating: (a) MWIR1; (b) MWIR2; and (c) LWIR1; and $t = 4$ s during square pulse heating (d) LWIR2. The scales were inverted in all cases in order to improve underdrawings visibility.

disappear at longer times. Apparently, the carbon-based underdrawings warm up (and cool down) at a faster rate than the painting layers. Hence, they are able to emit through the superficial painting layers at early times. After a few seconds though, they cool down while the painting layers conserve the heat longer being able to emit enough thermal radiations to hide those from the under-drawings.

This could mean that under-drawings are visible in these cases not because of reflection/transmission differences between the painting's layers and the under-drawings as was the case for the IR reflectography results previously presented, but because of the thermal differences between materials (charcoal sketches *vs.* white ground).

To confirm this, a 30×20 cm heating plate was used as an illuminator, emitting radiant energy mainly in the MWIR and LWIR bands. Electrical power was set to the minimum and the plate was placed several meters from the specimen to avoid heating the painting. In this manner, only reflected energy in the MWIR and LWIR is captured by the camera (and no thermal emissions). The MWIR thermogram in Fig. 9(a) shows some indications of under-drawings and surface painting, whilst the LWIR thermogram Fig. 9(b) does not show anything at all. This is probably due to a superior detector performance of the MWIR2 camera with respect to the LWIR1 microbolometer measured as noise equivalent temperature difference (NEdT), i.e. 25 mK *vs.* 60 mK. An interesting experiment would be to obtain a reflectogram with a cooled LWIR camera (NEdT ~25 mK). It can be concluded that under-drawing visibility in the MWIR and LWIR is mostly due to thermal differences, similar to NIR and SWIR reflectograms with some small contribution from possible light reflections in the case of MWIR.

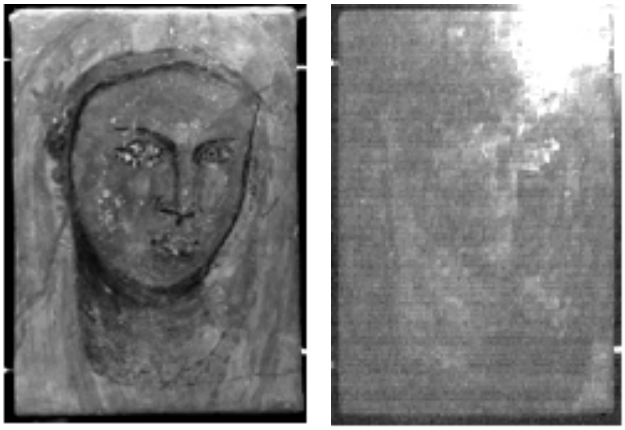

(a) MWIR2 (b) LWIR1

Fig. 9. Mid- and long-wave IR reflectograms obtained using an illuminator in the MWIR or LWIR: (a) MWIR2; and (b) LWIR1.

As a last observation, it is interesting to note that active IR thermography, using a MWIR or a LWIR camera, besides the characterization of internal defects (delaminations), would allow the inspection of paintings for the detection of under-drawings. It should be pointed out, however, that NIR/SWIR reflectography still provides better results (underdrawings appear with better contrast) than active thermography, as can be confirmed from comparison of Fig. 4 and 5 (reflectography) to Fig. 8 (thermography).

3.6. Terahertz spectrum (100 to 1000 μm)

The terahertz spectrum is located between the wavelengths of 100 and 1000 μm. Nevertheless, it is usually denoted in terms of frequency, instead of wavelength. The equivalent frequencies are located between 0.3 and 3 THz, although the commonly accepted range for THz goes from 0.1 to 5 THz.

Terahertz results are presented in Fig. 10. In all cases, a frequency of 0.11 THz (i.e., very close to the lower limit of the THz spectrum) and a scanning resolution of 3 mm were used. Fig. 10(a) was obtained in a transmission mode and shows several features. Firstly, the contour between the face and the headscarf of *The Madonna* can be distinguished in the top right corner, as indicated. Secondly, there are several regions showing a loss of signal that might indicate the presence of defects. Some of them match, more or less, the locations of actual artificial defects. For instance, the one at the bottom left corner, which relates to a Mylar rectangular insert [defect B in Fig. 7(b)]. The location of another interesting feature is highlighted with a black circle; it is close to the location of a circular Mylar insert reported by the manufacturer of the painting [defect D in Fig. 7(b)]. Interestingly,

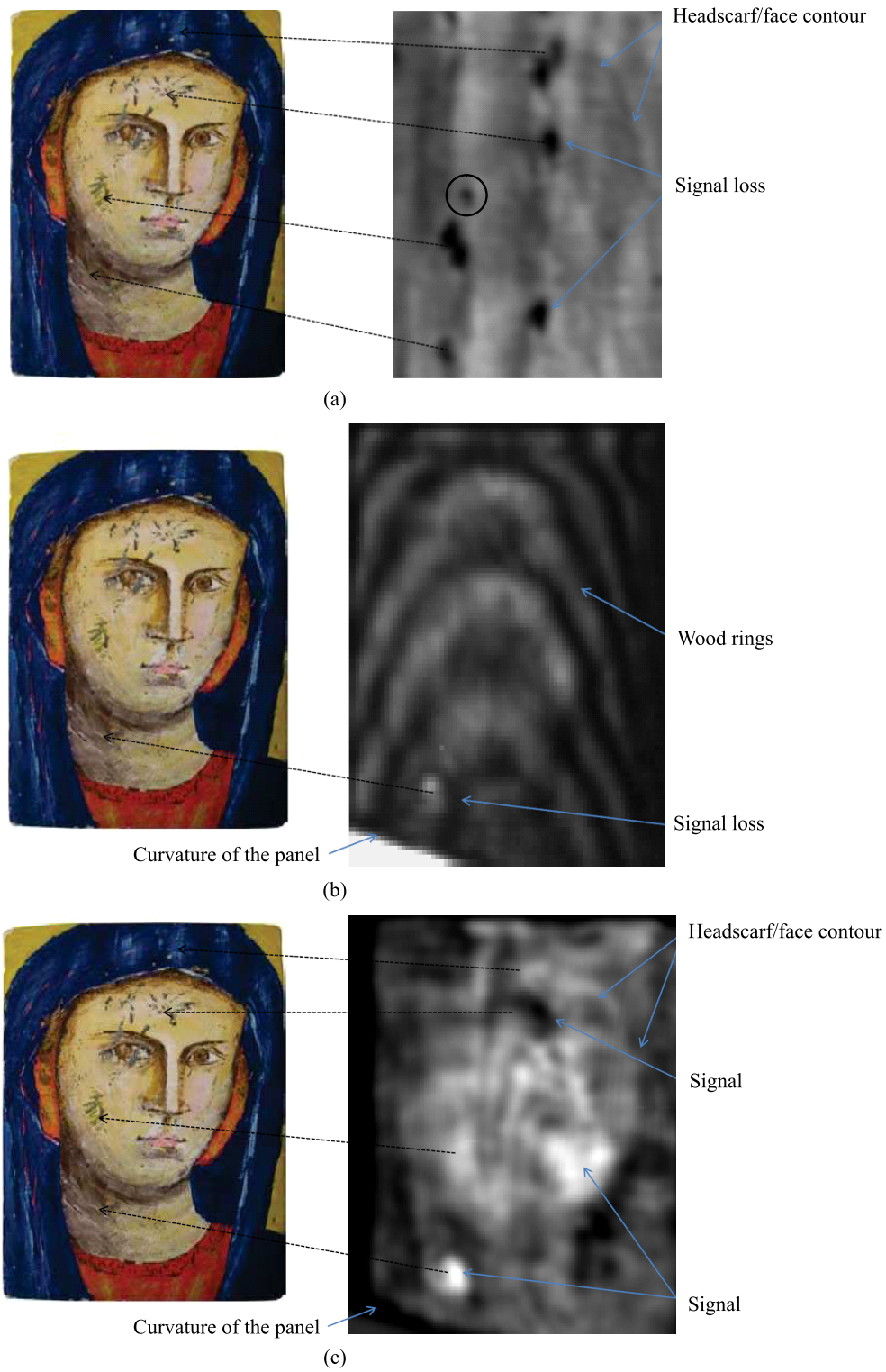

Fig. 10. Terahertz imaging results, (frequency = 0.11 THz, resolution = 3 mm): (a) transmission mode; (b) normal reflection; and (c) oblique reflection.

this defect was not detected by active thermography [21,22] nor by holographic interferometry [22,23].

Fig. 10(b) was produced in normal reflection mode; it provides more information about the wood support (rings), and it is possible to see an indication of defect B [Fig. 7(b)] in the bottom left corner.

Finally, Fig. 10(c) obtained in an oblique reflection mode, shows information about shallower features than Fig. 10(b). The face/headscarf contour is visible as in the case of the transmission image, as well as defect B [Fig. 7(b)]. However, there are two additional regions whose origin is difficult to explain. One shows a loss of signal (bright re-

gion at the centre-right) and another one showing an increased terahertz signature (dark area at the centre-top).

In order to improve terahertz imaging results, it would be required to use higher frequencies, such as 0.24 THz, or even 2 THz, and to employ higher scanning resolutions.

4. Conclusions

A multispectral subsurface imaging approach was investigated herein for the inspection of a panel painting with under-drawings and some hidden defects. The investigated spectral range goes from the UV to the THz. The UV image at 400 nm is quite interesting since it shows gold tones very clearly. Other than the slight indication of the hidden signature, the rest of the UV images do not appear to provide remarkable results. NIR/SWIR reflectograms are more interesting. It was observed that, in accordance with previously published works, transparency in the IR spectrum improves from the NIR to the SWIR bands. The statement that a peak of transparency around 2000 nm could not be fully confirmed however, since there is a gap between 1.7 and 3 μm (1700–3000 nm) in the operation spectral band of the equipment available for this research. Nevertheless, it was observed that the reflectograms showing underdrawings with the most enhanced contrast correspond to the SWIR band (1300, 1430, and 1650 nm). The reflectograms obtained in the MWIR and LWIR bands presented a notable reduction in contrast.

Interestingly, under-drawings can also be detected from active IR thermography experiments, especially at the beginning of the cooling process, i.e., right after heating. These images correspond actually to emissivity maps (thermograms) in the MWIR/LWIR bands as demonstrated from a subsequent set of experiments using an exclusively radiant heat source from which actual reflectograms were obtained. The resulting thermograms only showed slight indications of the under-drawings thermal signature. Hence, active IR thermography inspection could be considered for the simultaneous detection of subsurface defects (delaminations) and underdrawings when NIR/SWIR reflectography equipment is not available. The latter or the thermal quasi-reflectography technique, however, will still provide better details of under-drawings [33].

Terahertz inspection was produced in normal and oblique reflection mode, as well as in transmission mode, providing information about the wood support (rings), Mylar insert, and shallower features. The face/headscarf contour is visible both in reflection and in transmission mode, although two additional regions require more analysis in order to establish their origin. This technique was the only one capable of detecting a defect [defect D in Fig. 7(b)] close to the circular Mylar insert, not detected by active thermography nor by holographic interferometry in the previous works reported in the references [18–23].

Future work includes the exploration of the 1.7 μm–3 μm range using the proper equipment, to investigate the use of a cooled LWIR camera with NEdT < 25 mK using a radiant heat source, and to employ higher frequencies (e.g., 0.24 or 2 THz) and/or higher scanning resolutions for THz imaging.

References

1. J. Desneux, "Underdrawings and pentimenti in the pictures of Jan Van Eyck", *The Art Bulletin* **40**, 13–21 1958.
2. E. Walmsley, C. Metzger, J.K. Delaney, and C. Fletcher, "Improved visualization of underdrawings with solid-state detectors operating in the infrared", *Stud. Conserv*. **39**, 217–231 (1994).
3. C. Daffara, E. Pampaloni, L. Pezzati, M. Barucci, and R. Fontana, "Scanning multi-spectral IR reflectography SMIRR: an advanced tool for art diagnostics", *Acc. Chem. Res*. **43,** 1–15 (2010).
4. D. Ambrosini, C. Daffara, R. Di Biase, D. Paoletti, L. Pezzati, R. Bellucci, and F. Bettini, "Integrated reflectography and thermography for wooden paintings diagnostics", *J. Cult. Herit*. **11**, 196–204 (2010).
5. M. Gargano, N. Ludwig, and G. Poldi, "A new methodology for comparing IR reflectographic systems", *Infrared Phys. Techn*. **49,** 249–353 (2007).
6. J.R.J. Van Asperen de Boer, "Infrared Reflectograms of panel paintings", *Stud. Conserv*. **11**, 45–46 (1966).
7. J.R.J. Van Asperen de Boer, "Reflectography of paintings using an infrared vidicon television system", *Stud. Conserv*. **14**, 96–118 (1969).
8. Rijksmuseum, Infrared reflectography, [online] ttp://www.rijksmuseum.nl/aria/aria_encyclopedia/00047885?lang=en, accessed on May 21, 2009.
9. The Cleveland Museum of Art, Infrared reflectography, [online] ttp://www.clevelandart.org/ exhibcef/picassoas/htmlk/7464063.html, accessed on May 21, 2009.
10. The Art Institute of Chicago, Examination techniques, [online] ttp://www.artic.edu/aic/conservation/revealingpicasso/exam_infared.html, accessed on May 21, 2009.
11. A.E. Obrutsky and D. Acosta, Reflectography: an NDT method for images diagnosis, in: NDT.net Ed., *Proc. of WCNDT – World Conference on Nondestructive Testing,* [CD-rom], 16th Edition, Montreal, [available online:http://www.ndt.net/article/wcndt2004/pdf/optical_techniques/740_obrutsky.pdf], 2004.
12. A. Aldrovandi, D. Bertani, M. Cetica, M. Matteini, A. Mole, P. Poggi, and P. Tiano, "Multispectral image processing of paintings", *Stud. Conserv*. **33**, 154–159 (1988).
13. R.B. Dinwiddie and S.W. Dean, "Case study of IR reflectivity to detect document the underdrawing of a 19th Century oil painting", *Proc. SPIE* **6205** 6205101–62051012 (2006).
14. K. Nicolaus, *The Restoration of Paintings*, Konemann, Cologne, 1998.
15. M.F. Mecklenburg, C.S. Tumosa, and D. Erhardt, "Structural response of painted wood surfaces to changes in ambient relative humidity", in: *Proc. of painted wood: history and conservation*, V. Dorge, F. Carey Howlett eds., Williamsburg, VA, [available online:http://www.getty.edu/conservation/publications/pdf_publications/books.html], 1994.
16. C. Cennini, *Il Libro Dell'arte, Revised Edition*, The Craftsman, English translation by D.V. Thompson Jr., Dower, N.Y., 1971.
17. E. Kouloumpi, A.P. Moutsatsou, M. Trompeta, J. Olafsdottir, C. Tsaroucha, A.V. Terlixi, R.M. Groves, M. Georges,

G.M. Hustinix, and V. Tornari, "Laser-based structural diagnosis: a museum's point of view", in: M. Castillejo, P. Moreno, M. Oujja, R. Radvan, J. Ruiz eds., *Lasers in the Conservation of Artworks*, P.O. Moore ed., 7th edition, Taylor & Francis, pp. 407–411, London, 2008.
18. G. Schirripa Spagnolo, D. Ambrosini, and D. Paoletti, "Image decorrelation for in situ diagnostics of wooden artifacts", *Appl. Opt*. **36**, 8358–8362 (1997).
19. G. Schirripa Spagnolo, D. Ambrosini, and D. Paoletti, "Comparative study on the efficiency of some optical methods for artwork diagnostics", *Proc. SPIE* **4402**, 227–234 (2001).
20. C. Ibarra-Castanedo, S. Sfarra, D. Ambrosini, D. Paoletti, A. Bendada, and X.P. Maldague, "Infrared vision for the nondestructive assessment of panel paintings", *CINDE J.* **31**, 5–9 (2010).
21. E. Grinzato, S. Marinetti, V. Vavilov, and P.G. Bison, "Non-destructive testing of wooden painting by IR thermography", *Proc. 8th – European Conf. Nondestructive Testing*, Barcelona, Spain, 2002.
22. C. Ibarra-Castanedo, S. Sfarra, D. Ambrosini, D. Paoletti, A. Bendada, and X.P. Maldague, "Diagnostics of panel paintings using holographic interferometry and pulsed thermography", *Quantitative Infrared Thermography J.* **7**, 85–114 (2010).
23. D. Ambrosini, D. Paoletti, and G. Galli, "Integrated digital speckle techniques for artworks monitoring", in: M. Castillejo, P. Moreno, M. Oujja, R. Radvan, J. Ruiz eds., *Lasers in the Conservation of Artworks*, P.O. Moore ed., 7th edition, Taylor & Francis, London, 2008.
24. M. Hain, J. Bartl, and V. Jacko, "Multispectral analysis of cultural heritage artefacts", *Meas. Sci. Rev*. **3**, 9–12 (2003).
25. R.M. Groves, B. Pradarutti, E. Kouloumpi, W. Osten, G. Notni, "2D and 3D non-destructive evaluation of a wooden panel painting using shearography and terahertz imaging", *NDT&E Int*. **42**, 543–549 (2009).
26. X.P.V. Maldague, *Theory and Practice of Infrared Technology for Nondestructive Testing*, John Wiley & Sons, N.Y., 2001.
27. R.L. Crane, "Aerospace applications of infrared and thermal testing: Part 3. pulsed thermal inspection of aging aircraft", in: X. Maldague technical ed., P.O. Moore ed., Nondestructive Handbook, *Infrared and Thermal Testing*, Vol. **3**, Chapter 15, 3rd edition, ASNT Press, Columbus, 2001.
28. P. Theodorakeas, C. Ibarra-Castanedo, S. Sfarra, N.P. Avdelidis, M. Koui, X. Maldague, D. Paoletti, and D. Ambrosini, "NDT inspection of plastered mosaics by means of transient thermography and holographic interferometry", *NDT&E Int*. **47**, 150–156 (2012).
29. R.W. Arndt, "Square pulse thermography in frequency domain as adaptation of pulsed phase thermography for qualitative and quantitative applications in cultural heritage and civil engineering", *Infrared Phys. Techn*. **53**, 246–253 (2010).
30. N.P. Avdelidis and A. Moropoulou, "Applications of infrared thermography for the investigation of historic structures (Review)", *J. Cult. Herit*. **5**, 119–127 (2004).
31. X. P. Maldague and S. Marinetti, "Pulse phase infrared thermography", *J. Appl. Phys*. **79**, 2694–2698 (1996).
32. S. Sfarra, P. Theodorakeas, C. Ibarra-Castanedo, N.P. Avdelidis, A. Paoletti, D. Paoletti, K. Hrissagis, A. Bendada, M. Koui, and X. Maldague, "Evaluation of defects in panel paintings using infrared, optical and ultrasonic techniques", *Insight* **54**, 21–27 (2012).
33. C. Daffara, D. Ambrosini, L. Pezzati, and D. Paoletti, "Thermal quasi-reflectography: a new imaging tool in art conservation", *Opt. Express* **20**, 14746–14753 (2012).